

Cite this: *Dalton Trans.*, 2018, **47**, 11455

Experimental and theoretical exploration of magnetic exchange interactions and single-molecule magnetic behaviour of bis(η^1 : η^2 : μ_2 -carboxylate) Gd_2^{III}/Dy_2^{III} systems†

Sagar Ghosh,^a Shuvankar Mandal,^a Mukesh Kumar Singh,^b Cai-Ming Liu,^c Gopalan Rajaraman^{b*} and Sasankasekhar Mohanta^{b*}

The present report deals with the syntheses, crystal structures, dc/ac magnetic properties and DFT/*ab initio* CASSCF calculations of two isomorphous bis(η^1 : η^2 : μ_2 -acetate) Gd_2^{III}/Dy_2^{III} compounds of the formula $[Ln_2^{III}L_2(\text{acetate})_4(\text{MeOH})_2]$ (**1**, Ln = Gd; **2**, Ln = Dy), where HL is (*E*)-*N'*-(3-ethoxysalicylidene)acetohydrazide. The two lanthanide(III) centres in each compound are symmetry-related owing to the presence of an inversion centre. Both compounds exhibit intramolecular ferromagnetic exchange interactions. The Dy_2^{III} analogue is a single-molecule magnet (SMM) with $U_{\text{eff}} = 52.8 \text{ cm}^{-1}$ and $\tau_0 = 1.52 \times 10^{-6} \text{ s}$. DFT calculations for **1** and *ab initio* calculations for **2** also reveal ferromagnetic interactions. *Ab initio* calculations of the SMM behaviour of **2** and two other reported and structurally related compounds reveal the importance of the weak exchange interaction present between the two Dy^{III} ions, and a relaxation mechanism has been developed to take into account the magnetic exchange interaction and to rationalize the observed difference in the U_{eff} values.

Received 17th May 2018,

Accepted 16th July 2018

DOI: 10.1039/c8dt02008f

rsc.li/dalton

Introduction

High unquenched orbital angular momentum gives rise to strong anisotropy in most lanthanides, and, taking advantage of this strong anisotropy, people have used lanthanides in magnetism for a long period; for example, the strongest known magnets, namely, SmCo_5 and $\text{Nd}_2\text{Fe}_{14}\text{B}$, are alloys that contain lanthanides.¹ However, the magnet-like behaviour of lanthanides at a molecular level was first reported 15 years ago in 2003, when Ishikawa *et al.* reported the single-molecule magnet (SMM) behaviour of tetrabutylammonium bis(phthalocyanine)terbiumate(III), with an energy barrier of magnetization reversal (U_{eff}) of 230 cm^{-1} ,² which is much higher than the U_{eff} values of numerous 3d SMMs that have been reported since the discovery of slow relaxation of magnetism

in an $\text{Mn}^{III}\text{Mn}^{IV}$ cluster in the early 1990s.³ Although SMMs have potential applications in advanced technological areas such as molecular spintronics,⁴ qubits,^{4a,5} and ultrahigh-density magnetic information storage,^{3b,6} their blocking temperature (T_B) and U_{eff} value should be greatly enhanced for any practical applications, and lanthanides are the ideal candidates for achieving this. Therefore, the first report of a lanthanide SMM was followed by a great number of SMMs containing lanthanides, which included mono/di/oligonuclear and polymeric 4f systems,^{1c,d,7–19} as well as 3d–4f compounds^{7g,20–26} of various nuclearities. It has been realized that Dy^{III} is the best lanthanide for achieving high T_B and U_{eff} values because of the combination of three favourable factors: the bistable nature of the ground state irrespective of the ligand field, significant magnetic anisotropy and a large magnetic moment.^{1c,d,7,8} It has also been realized that lanthanide compounds of low nuclearities (in particular, mononuclear compounds) should be better SMMs, as the magnetic exchange interactions involving 4f orbitals are very weak. In particular, a blocking temperature of as high as 60 K has been achieved recently in a mononuclear dysprosium(III) compound.^{8a}

Although a renaissance has been continuing in the field of lanthanide SMMs, two other important aspects of molecular magnetism, namely, magnetic exchange interactions and magneto-structural correlations,^{27–32} have been little investi-

^aDepartment of Chemistry, University of Calcutta, 92 A. P. C. Road, Kolkata 700009, India. E-mail: sm_cu_chem@yahoo.co.in

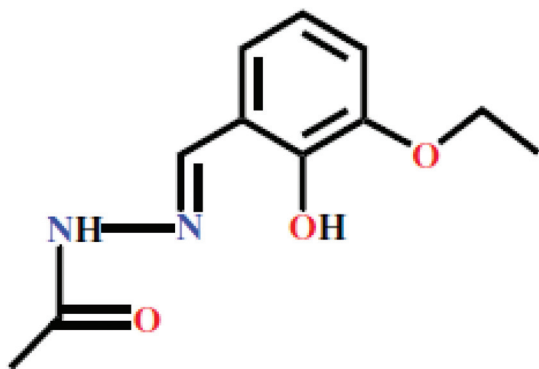
^bDepartment of Chemistry, Indian Institute of Technology Bombay, Powai, Mumbai 400076, India. E-mail: rajaraman@chem.iitb.ac.in

^cBeijing National Laboratory for Molecular Sciences, Centre for Molecular Science, Institute of Chemistry, Chinese Academy of Sciences, Beijing 100190, PR China

† Electronic supplementary information (ESI) available: Details of structural and magnetic data. CCDC 1843779 and 1843780 for **1** and **2**. For ESI and crystallographic data in CIF or other electronic format see DOI: 10.1039/c8dt02008f

gated in lanthanide systems,^{30–32} particularly in anisotropic lanthanides.³² One reason for this lack of research is definitely the deep-seated nature of the 4f orbitals and the associated very weak exchange interactions. A second reason is the difficulty of understanding even the nature of the exchange interactions, because the profile of the product of susceptibility and temperature *versus* temperature is dominated by the variation in the population of the Stark levels. A third reason is the expected insignificant influence of the variation in ligands on the magnetic exchange interactions of closely similar compounds. As a result, studies of magnetic exchange interactions as a function of structural parameters or the transition between antiferromagnetic and ferromagnetic exchange interactions in closely similar lanthanide compounds are too scarce.³²

There is no doubt that studies of both slow relaxation of magnetization and the transition between ferromagnetic and antiferromagnetic interactions in lanthanide compounds deserve attention, and dilanthanide compounds are the best systems for such simultaneous investigations. It is worth mentioning that the study of the single-molecule magnet properties (*e.g.*, the anisotropic energy barrier, pathways of relaxation, *etc.*) of lanthanide compounds by *ab initio* calculations and electrostatic analyses is a popular topic in molecular magnetism.^{8b,d,9b,c,10b,11a–c,12c,15a,b,16a,b,20a,22a,b,24a,b,25a,32} In a number of low-nuclearity lanthanide systems, magnetic exchange interactions have also been modelled by *ab initio* calculations.^{11a–c,12c,15a,b,16a,b,20a,22a,b,24a,b,25a,32} With the aim of studying SMM properties and magnetic exchange interactions, we prepared two bis(η^1 : η^2 -acetate) $\text{Dy}^{\text{III}}/\text{Gd}^{\text{III}}$ compounds of the formula $[\text{Ln}^{\text{III}}\text{L}_2(\text{acetate})_4(\text{MeOH})_2]$ (**1**, Ln = Gd; **2**, Ln = Dy), where HL is (*E*)-*N'*-(3-ethoxysalicylidene)acetohydrazide (Scheme 1). The Dy^{III} analogue is an SMM, and both compounds exhibit ferromagnetic interactions, whereas the few existing examples that have a similar bridging moiety are known to exhibit antiferromagnetic interactions.¹² The present report describes the syntheses, crystal structures, dc/ac magnetic properties and DFT/*ab initio* magnetic properties of **1** and **2**, together with *ab initio* calculations for some previously reported related systems.



Scheme 1 Chemical structure of the ligand HL.

Experimental section

Materials and physical measurements

All reagents and solvents were purchased from commercial sources and were used as received. Elemental (C, H and N) analyses were performed using a PerkinElmer 2400 II analyzer. IR spectra were recorded in the region of 400–4000 cm^{-1} using a Bruker Optics Alpha-T spectrophotometer with samples as KBr disks. The dc magnetic susceptibility data at a constant field strength of 0.1 T of **1** and **2** and dc magnetization data of **2** in the temperature range of 2.5–10 K were recorded with a SQUID-VSM (Quantum Design) instrument, whereas all other dc/ac magnetic measurements were performed using a Quantum Design MPMS-XL5 SQUID magnetometer. Diamagnetic corrections were performed on the basis of Pascal's constants.

Syntheses

HL. A solution of acetohydrazide (0.37 g, 5 mmol) in 15 mL ethanol was added dropwise to a 25 mL ethanolic solution of 3-ethoxysalicylaldehyde (0.83 g, 5 mmol) under warm conditions. The reaction mixture was refluxed for 1 h. After cooling, the volume of the solution was reduced to 20 mL under vacuum. The resulting pale yellow solution was then kept overnight. After one day, the white crystalline compound, namely, HL, that was deposited was collected by filtration and washed with ethanol. Yield: 0.73 g (66%).

$[\text{Ln}^{\text{III}}\text{L}_2(\text{acetate})_4(\text{MeOH})_2]$ (**1**, Ln = Gd; **2**, Ln = Dy). These two compounds were prepared by following the general procedure as follows: a methanolic solution (5 mL) of the corresponding hydrated $\text{Ln}(\text{acetate})_3$ (0.5 mmol) and a methanolic solution (5 mL) of Et_3N (0.05 g, 0.5 mmol) were added dropwise successively to a 25 mL methanolic solution of HL (0.11 g, 0.5 mmol) under stirring. The resulting yellow solution was stirred for 3 h and then filtered to remove some suspended particles. The volume was reduced to *ca.* 5 mL on a rotary evaporator. The reduced solution was filtered into a long tube. To the yellow filtrate, diethyl ether was added very slowly to make two separate layers, and the tube was made airtight and kept undisturbed. A few days later, yellow single crystals of X-ray diffraction quality were separated, which were collected by filtration and washed with cold methanol.

Data for **1**: Yield: 0.16 g (60%). Anal. Calc. for $\text{C}_{32}\text{H}_{46}\text{N}_4\text{O}_{16}\text{Gd}_2$ (FW: 1057.23): C, 36.35; H, 4.39; N, 5.30. Found: C, 36.17; H, 4.44; N, 5.21%. Selected FT-IR data (KBr, cm^{-1}): $\nu(\text{O-H})$, 3290 w; $\nu(\text{C=N})$, 1617 s; $\nu_{\text{as}}(\text{CO}_2^-)$, 1563 vs.; $\nu_{\text{s}}(\text{CO}_2^-)$, 1444 s.

Data for **2**: Yield: 0.16 g (60%). Anal. Calc. for $\text{C}_{32}\text{H}_{46}\text{N}_4\text{O}_{16}\text{Dy}_2$ (FW: 1067.73): C, 36.00; H, 4.34; N, 5.25. Found: C, 36.31; H, 4.25; N, 5.36%. Selected FT-IR data (KBr, cm^{-1}): $\nu(\text{O-H})$, 3284 w; $\nu(\text{C=N})$, 1618 s; $\nu_{\text{as}}(\text{acetate})$, 1563 vs.; $\nu_{\text{s}}(\text{acetate})$, 1444 s.

Crystal structure determination for **1** and **2**

The crystallographic data of compounds **1** and **2** are summarized in Table 1. Diffraction data for two crystals were recorded

Table 1 Crystallographic data for 1 and 2

	1	2
Empirical formula	C ₃₂ H ₄₆ N ₄ O ₁₆ Gd ₂	C ₃₂ H ₄₆ N ₄ O ₁₆ Dy ₂
Formula weight	1057.23	1067.73
Crystal system	Monoclinic	Monoclinic
Space group	<i>P</i> 2 ₁ / <i>n</i>	<i>P</i> 2 ₁ / <i>n</i>
<i>a</i> /Å	11.4479(7)	11.4531(5)
<i>b</i> /Å	13.9987(9)	13.9589(6)
<i>c</i> /Å	13.0690(8)	13.0023(5)
α /°	90.00	90.00
β /°	108.991(2)	108.982(2)
γ /°	90.00	90.00
<i>V</i> /Å ³	1980.4(2)	1965.67(14)
<i>Z</i>	2	2
ρ_{calcd} /g cm ⁻³	1.773	1.804
λ (Mo K α)/Å	0.71073	0.71073
μ /mm ⁻¹	3.393	3.846
<i>T</i> /K	296(2)	296(2)
<i>F</i> (000)	1044	1052
2 θ range for data collection (°)	4.12–54.20	4.12–53.72
Index ranges		
	–13 ≤ <i>h</i> ≤ 14	–14 ≤ <i>h</i> ≤ 14
	–16 ≤ <i>k</i> ≤ 17	–17 ≤ <i>k</i> ≤ 17
	–16 ≤ <i>l</i> ≤ 16	–14 ≤ <i>l</i> ≤ 16
No. measured reflections	24 420	28 225
No. independent reflections	4312	4220
<i>R</i> _{int}	0.0594	0.0688
No. refined parameters	257	257
No. observed reflections, <i>I</i> ≥ 2 σ (<i>I</i>)	3187	3299
Goodness of fit on <i>F</i> ² , <i>S</i>	0.937	0.952
<i>R</i> ₁ ^a , <i>wR</i> ₂ ^b [<i>I</i> ≥ 2 σ (<i>I</i>)]	0.0324, 0.0770	0.0315, 0.0780
<i>R</i> ₁ ^a , <i>wR</i> ₂ ^b (all data)	0.0527, 0.0883	0.0457, 0.0863

$$^a R_1 = [\sum ||F_o| - |F_c|| / \sum |F_o|]. \quad ^b wR_2 = [\sum w(F_o^2 - F_c^2)^2 / \sum w(F_o^2)^2]^{1/2}.$$

at 296 K with a Bruker APEX II SMART CCD diffractometer using graphite-monochromated Mo K α radiation ($\lambda = 0.71073$ Å). The SAINT^{33a} and SADABS^{33b} packages were used for data processing and absorption corrections. The structures were solved by direct and Fourier methods and refined by full-matrix least-squares based on *F*² using the SHELXL-97^{33c} and SHELXL-2014/7^{33d} packages.

All hydrogen atoms in 1 and 2 were inserted at calculated positions with isotropic thermal parameters and refined freely. All non-hydrogen atoms were refined anisotropically, whereas all hydrogen atoms were refined isotropically. The final refinement converged at *R*₁ [*I* > 2 σ (*I*)] values of 0.0324 and 0.0315 and *wR*₂ [*I* > 2 σ (*I*)] values of 0.0770 and 0.0780 for 1 and 2, respectively.

Results and discussion

Description of crystal structures of 1 and 2

Compounds 1 and 2 crystallize in the monoclinic crystal system and *P*2₁/*n* space group with practically identical values of the unit cell parameters (Table 1), which reveals that these two compounds are isomorphs. They have similar formulae, namely, [Ln^{III}L₂(acetate)₄(MeOH)₂] (Ln = Gd for 1 and Dy for 2), and similar internal structures, as shown in Fig. 1 and 2. Both are dilanthanide(III) compounds in which the metal ions

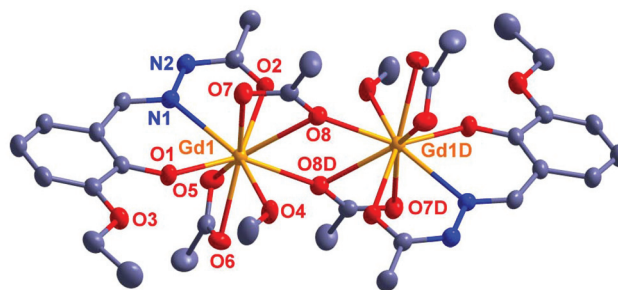


Fig. 1 ORTEP drawing (ellipsoid probability of 30%) of [Gd₂L₂(OAc)₄(MeOH)₂] (1). Hydrogen atoms are omitted for clarity. Symmetry code: D, 1 – *x*, 2 – *y*, 1 – *z*.

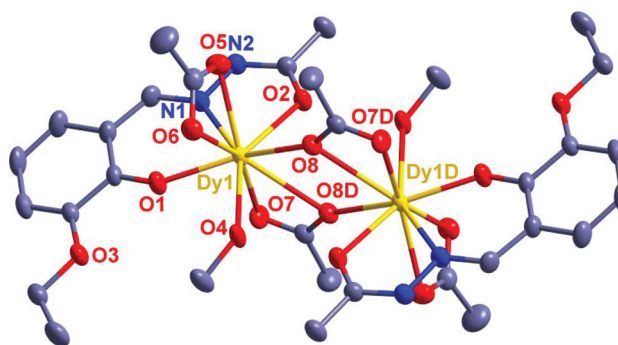


Fig. 2 ORTEP drawing (ellipsoid probability of 30%) of [Dy₂L₂(OAc)₄(MeOH)₂] (2). Hydrogen atoms are omitted for clarity. Symmetry code: D, –*x*, –*y*, –*z*.

are coordinated to two deprotonated hydrazide ligands L[–], four acetate ligands and two methanol molecules. One half of each structure is symmetry-related to the other half owing to the presence of an inversion centre. Of the two pockets/compartments of the L[–] ligand, the O(phenolate)N(hydrazono)O (carboxyl) pocket (O1N1O2) accommodates a lanthanide(III) centre, whereas the other pocket, *i.e.*, the O(phenolate)O (ethoxy) compartment (O1O3), is vacant because the ethoxy oxygen atom remains non-coordinated. Each metal ion is also coordinated to the oxygen atom (O4) of a methanol molecule, two oxygen atoms (O5 and O6) of η²-acetate ligands, and three oxygen atoms (O7, O8 and O8D) of two symmetry-related η¹:η²:μ₂-acetate moieties. As a result, the two metal ions, namely, Gd1/Dy1 and Gd1D/Dy1D, are bridged by two oxygen atoms (O8 and O8D) of two η¹:η²:μ₂-acetate ligands, *i.e.*, the two metal ions are effectively bridged by a bis(μ_{1,1}-acetate) moiety.

Evidently, the lanthanide ions in 1/2 are nine-coordinated by one nitrogen and eight oxygen atoms, with the Ln–O/N bond distances lying in the ranges of 2.224(3)–2.621(3) Å and 2.193(3)–2.650(3) Å for 1 and 2, respectively (Table 2). The ranges of the O/N–Ln–O/N bond angles (50.65(10)–152.80(12)° in 1; 50.53(10)–152.88(12)° in 2), the metal...metal separation in the dinuclear unit (4.25 Å in both compounds) and the metal–phenoxo–metal bridge angle (114.82(12)° in 1; 115.36(12)° in 2) in the two compounds are practically identical

Table 2 Selected structural parameters (lengths in Å and angles in °) around the Ln^{III} centres in **1** and **2**. Symmetry code: D, 1 - x, 2 - y, 1 - z for **1** and -x, -y, -z for **2**

	Ln = Gd (1)	Ln = Dy (2)
Bond lengths		
Ln1-O1	2.224(3)	2.193(3)
Ln1-O2	2.427(3)	2.405(3)
Ln1-N1	2.547(4)	2.530(3)
Ln1-O4	2.404(3)	2.374(3)
Ln1-O5	2.458(3)	2.436(3)
Ln1-O6	2.468(3)	2.452(3)
Ln1-O7	2.452(4)	2.423(3)
Ln1-O8	2.621(3)	2.384(3)
Ln1-O8D	2.422(3)	2.650(3)
Bond angles		
O1-Ln1-N1	69.92(11)	70.26(12)
O1-Ln1-O2	132.36(11)	133.09(11)
O1-Ln1-O4	79.57(11)	79.37(11)
O1-Ln1-O5	96.89(12)	97.53(13)
O1-Ln1-O6	77.11(13)	77.02(13)
O1-Ln1-O7	81.23(12)	81.50(13)
O1-Ln1-O8	124.84(11)	148.03(11)
O1-Ln1-O8D	148.15(12)	124.77(12)
N1-Ln1-O2	63.53(11)	64.13(11)
N1-Ln1-O4	147.58(11)	147.77(12)
N1-Ln1-O5	68.96(12)	68.73(12)
N1-Ln1-O6	106.72(12)	106.52(11)
N1-Ln1-O7	80.60(12)	81.11(12)
N1-Ln1-O8	117.68(11)	136.42(11)
N1-Ln1-O8D	136.45(11)	118.14(10)
O2-Ln1-O4	141.85(10)	140.99(10)
O2-Ln1-O5	76.01(11)	76.18(11)
O2-Ln1-O6	125.15(12)	125.63(11)
O2-Ln1-O7	81.80(12)	81.32(12)
O2-Ln1-O8	72.28(10)	78.15(10)
O2-Ln1-O8D	78.57(10)	71.67(10)
O4-Ln1-O5	127.13(14)	127.44(13)
O4-Ln1-O6	75.85(13)	75.91(13)
O4-Ln1-O7	84.24(14)	84.06(14)
O4-Ln1-O8	71.42(11)	75.80(11)
O4-Ln1-O8D	75.97(11)	71.10(11)
O5-Ln1-O6	52.42(12)	52.81(11)
O5-Ln1-O7	147.97(13)	148.00(12)
O5-Ln1-O8	138.00(11)	82.22(11)
O5-Ln1-O8D	82.23(11)	137.46(11)
O6-Ln1-O7	152.80(12)	152.88(12)
O6-Ln1-O8	134.81(11)	77.65(12)
O6-Ln1-O8D	77.37(11)	134.51(10)
O7-Ln1-O8	50.65(10)	115.17(11)
O7-Ln1-O8D	115.82(11)	50.53(10)
O8-Ln1-O8D	65.18(12)	64.64(12)
Ln1-O8-Ln1D	114.82(12)	115.36(12)
Ln1...Ln1D	4.2501(4)	4.2563(4)

(Table 2). A SHAPE³⁴ analysis (Table 3) reveals that the most ideal geometry of the LnNO₈ coordination environment in both **1** and **2** is a spherical capped square antiprism (CSAPR), as shown in Fig. 3. In this coordination environment, a hydrazone nitrogen atom (N1), a phenolate oxygen atom (O1) and two η²-acetate oxygen atoms (O5 and O6) define a square plane, whereas the second square plane is defined by a carboxyl oxygen atom (O2), one bridging oxygen atom (O8 for Dy1 and O8D for Gd1), a methanol oxygen atom (O4) and the non-bridging oxygen atom (O7) of an η¹:η²:μ₂-acetate moiety. Clearly, the other bridging acetate oxygen atom (O8D for Dy1 and O8 for Gd1) is the capped atom.

Table 3 Results of continuous shape measures calculations for **1** and **2** performed using SHAPE v2.1³⁴

Compound	JCSAPR ^a	CSAPR ^a	TCTPR ^a	MFF ^a
1	2.318	1.790	2.861	1.887
2	2.168	1.787	2.895	1.900

^aJCSAPR = Capped square antiprism J10, CSAPR = Spherical capped square antiprism, TCTPR = Spherical tricapped trigonal prism, MFF = Muffin.

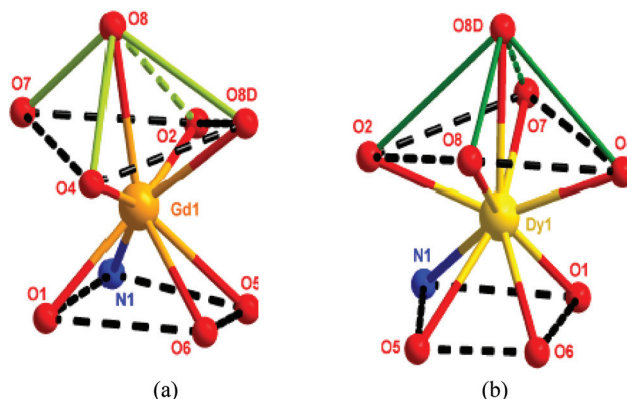


Fig. 3 Spherical capped square antiprismatic geometric environment of Gd^{III} center (a) and Dy^{III} center (b) in **1** and **2**, respectively.

There are three types of hydrogen bonds in both structures (Fig. S1 and S2; Table S1[†]). One of these bonds is intramolecular and involves the interaction of the hydroxy hydrogen atom (O4-H4A) of a coordinated methanol molecule and a carboxyl oxygen atom (O2). The other two (intermolecular) hydrogen bonds are formed between the following atoms: (i) one alkyl hydrogen atom (C12-H12B) of a coordinated methanol ligand in one molecule (first molecule) and one oxygen atom (O5F) of a chelating acetate moiety in another molecule (second molecule) and (ii) the N-H hydrogen atom (N2-H2A) of an L⁻ ligand in one molecule (first molecule) and one oxygen atom (O6E) of a chelating acetate moiety in another molecule (third molecule). Owing to the two types of intermolecular hydrogen bonds, one dinuclear molecule is interlinked with four other symmetry-related dinuclear molecules, which results in the generation of a two-dimensional sheet (Fig. S1 and S2[†]) in the structures of **1** and **2**. The geometries of the hydrogen bonds are listed in Table S1.[†]

Magnetic properties

The direct-current (dc) magnetic susceptibilities of both **1** and **2** at 0.1 T in the temperature range of 300–2 K are shown in Fig. 4 and 5, respectively, in the form of plots of χ_{MT} versus T . Data of M versus H for **1** at 2 K and **2** at 2.5, 4, 6, 8 and 10 K are shown in Fig. S3 and S4,[†] respectively, whereas data of M versus H/T for **2** are shown in Fig. 6.

The χ_{MT} value of **1** at 300 K is 15.72 cm³ K mol⁻¹, which is the same as the spin-only value expected for two non-corre-

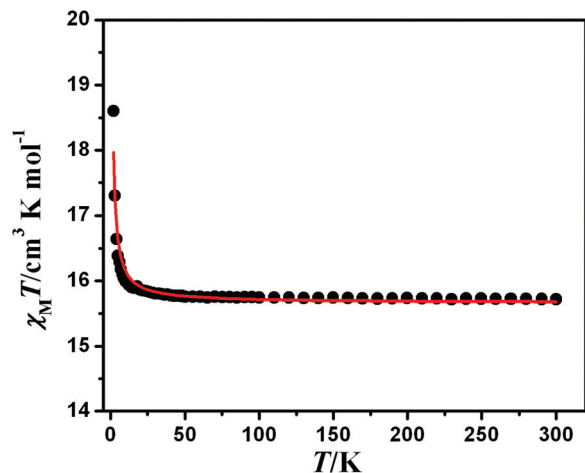


Fig. 4 Plot of $\chi_M T$ vs. T for $[\text{Gd}_2\text{L}_2(\text{OAc})_4(\text{MeOH})_2]$ (1) at 0.1 T. The solid red line corresponds to the best fit obtained using the *PHI* program.

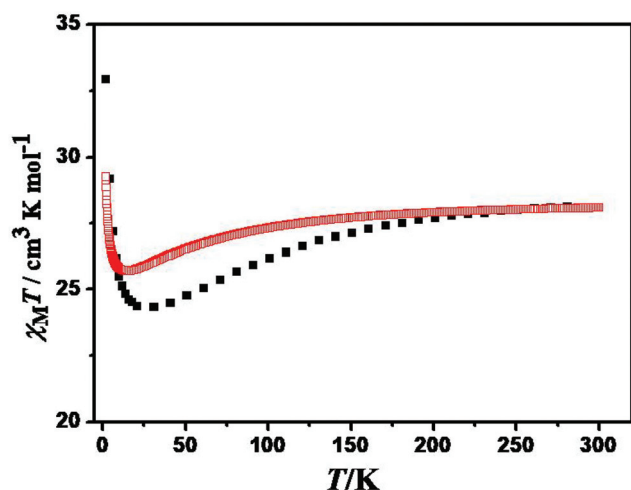


Fig. 5 Plot of $\chi_M T$ vs. T for $[\text{Dy}_2\text{L}_2(\text{OAc})_4(\text{MeOH})_2]$ (2) at 0.1 T. The black color indicates the experimental plot, whereas the red color indicates the plot computed using *POLY_ANISO*.

lated Gd^{III} ions with $S = 7/2$ and $g = 2.0$. On a decrease in temperature, $\chi_M T$ remains practically constant down to 15 K and then rapidly increases to $18.6 \text{ cm}^3 \text{ K mol}^{-1}$ at 2 K. The profile clearly indicates the existence of a weak ferromagnetic interaction between the two Gd^{III} centres in **1**. Taking $H = -2JS_1 \times S_2$ as the model Hamiltonian, the data for $\chi_M T$ versus T and M versus H were contemporaneously simulated using *PHI* software,³⁵ which gave the converging parameters $J = 0.021 \text{ cm}^{-1}$ and $g = 1.994$.

The $\chi_M T$ value of the Dy^{III} compound **2** at 300 K is $28.1 \text{ cm}^3 \text{ K mol}^{-1}$, which is very close to the theoretical value ($28.34 \text{ cm}^3 \text{ K mol}^{-1}$) expected for two non-correlated Dy^{III} ions with a $^6\text{H}_{15/2}$ ground state. On a decrease in temperature from 300 K, $\chi_M T$ decreases gradually to reach a minimum of $24.3 \text{ cm}^3 \text{ K mol}^{-1}$ at 30–20 K and then increases rapidly to $32.9 \text{ cm}^3 \text{ K mol}^{-1}$ at 2 K. The increase in $\chi_M T$ values below

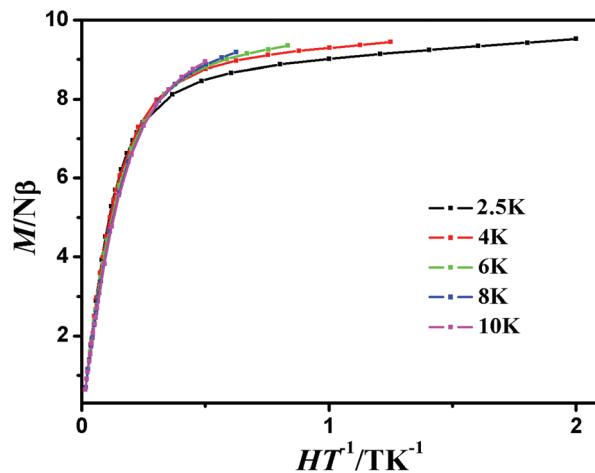


Fig. 6 Plots of M versus H/T for $[\text{Dy}_2\text{L}_2(\text{OAc})_4(\text{MeOH})_2]$ (2) at different temperatures.

20 K clearly indicates that the Dy^{III} centres in the Dy_2^{III} dinuclear unit are coupled by a ferromagnetic interaction. It is also evident that the decrease in $\chi_M T$ values in the temperature range of 300–30/20 K takes place owing to two inherent factors in Dy^{III} , namely, depopulation of the upper Stark sublevels and anisotropy, the latter of which can be confirmed from Fig. 6, where it is shown that the data of M versus H/T at different temperatures do not pass through a common master curve, and this, in turn, indicates that compound **2** has the potential to behave as a single-molecule magnet.

To study the dynamics of magnetization, in-phase (χ_M') and out-of-phase (χ_M'') ac susceptibilities in the temperature range of 20–2 K at different fixed frequencies (10, 25, 100, 250, 499, 651, 801, 997, and 1399 Hz; Fig. 7 and 8), as well as in the frequency range of 1–1488 Hz at different fixed temperatures (7, 8, 9, 10, 11, and 12 K; Fig. 9), were recorded under a zero dc field. As shown in Fig. 7 and 8, the variable-temperature data for both χ_M' and χ_M'' are not only frequency-dependent (below

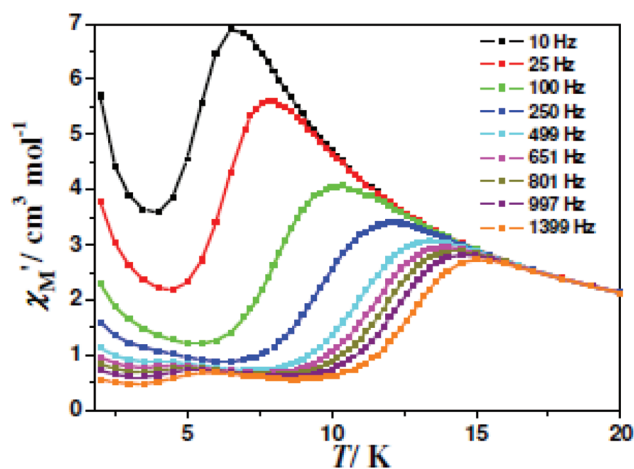


Fig. 7 Temperature dependence of the in-phase (χ_M') ac susceptibility of **2** under a zero dc field. The solid lines are used as guides for the eye.

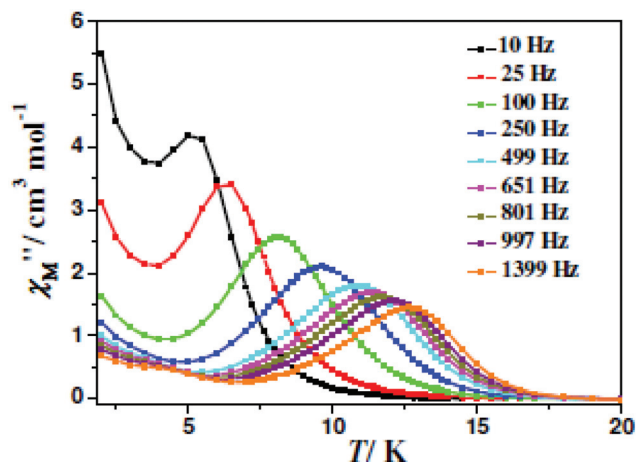


Fig. 8 Temperature dependence of the out-of-phase (χ_M'') ac susceptibility of **2** under a zero dc field. The solid lines are used as guides for the eye.

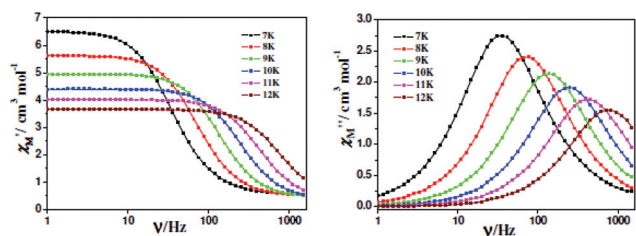


Fig. 9 Frequency dependence of the in-phase (χ_M') and out-of-phase (χ_M'') ac susceptibilities of **2** under a zero dc field. The solid lines are used as guides for the eye.

15 K and 17 K, respectively) but also exhibit sharp maxima in the ranges of 6.6–14.5 K and 5.3–12.7 K, respectively. As shown in Fig. 9, the variable-frequency data for both χ_M' and χ_M'' are temperature-dependent. All these results reveal that slow relaxation of magnetization takes place in **2**, and hence it is an SMM. Fitting of the temperature-dependent (12.7–8.2 K) out-of-phase data (Fig. 10) *via* multiple relaxation pathways using eqn (1) gives an energy barrier of $U_{\text{eff}} = 52.8 \text{ cm}^{-1}$ and $\tau_0 = 1.52 \times 10^{-6} \text{ s}$ *via* Raman ($C = 0.003 \text{ s}^{-1} \text{ K}^{-n}$ and $n = 5.67$) and QTM ($\tau_{\text{QTM}} = 0.032 \text{ s}$) processes.

$$\frac{1}{\tau} = \frac{1}{\tau_{\text{QTM}}} + CT^n + \frac{1}{\tau_0} \exp\left(\frac{-U_{\text{eff}}}{k_B T}\right) \quad (1)$$

Here, the three terms on the right-hand side represent relaxation *via* the QTM, Raman and thermally assisted Orbach relaxation mechanisms, respectively. However, below 8.2 K $\ln \tau$ is weakly dependent on temperature, which reveals the dominance of direct or phonon-promoted quantum tunnelling of magnetization, which is found to be the controlling factor in the lower-temperature region. Notably, the complex **2** does not exhibit any hysteresis even at 2 K (Fig. S5[†]), which indicates fast zero-field relaxation.

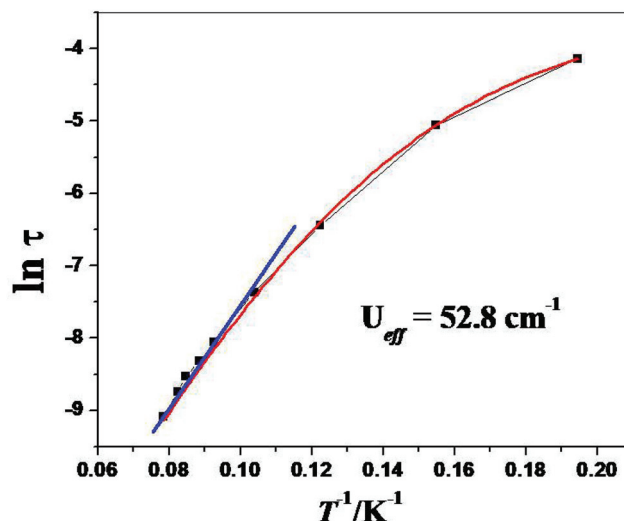


Fig. 10 Plot of the logarithm of the relaxation time $\ln \tau$ versus T^{-1} for **2** under a zero dc field. The solid lines represent fits *via* multiple relaxation pathways (see text for details).

A Cole–Cole plot (out-of-phase *versus* in-phase ac susceptibility data) in the temperature range of 7–12 K is shown in Fig. 11 and displays an asymmetrical semicircular shape. These data can be fitted with a generalized Debye model using CC-Fit software^{7f} to give values of the α parameter of less than 0.05 (Table S2[†]), which indicates a single relaxation pathway.

Previously, four Dy_2^{III} compounds with two $\eta^1:\eta^2:\mu_2$ -carboxylate moieties and a bis($\mu_{1,1}$ -carboxylate) bridging moiety have been reported, namely, $[\text{Dy}_2^{\text{III}}\text{L}^1_2(\text{acetate})_4(\text{MeOH})_2] \cdot 2\text{MeOH}$ (**3**; Scheme S3[†]),^{12a} $[\text{Dy}_2^{\text{III}}(n\text{-butyrate})_6(\text{MeOH})_2(\text{H}_2\text{O})_2]$ (**4**; Scheme S3[†]),^{12b} $[\text{Dy}_2^{\text{III}}(2,4'\text{-pcad})_2(\text{acetate})_4(\text{H}_2\text{O})_2] \cdot 4\text{H}_2\text{O}$ (**5**; Scheme S3[†])^{12c} and $[\text{Dy}_2^{\text{III}}(2,3'\text{-pcad})_2(\text{acetate})_4(\text{H}_2\text{O})_2]$ (**6**; Scheme S3[†]),^{12c} where $\text{HL}^1 = [E\text{-}N'(2\text{-hydroxybenzylidene})\text{-}2\text{-mercaptocotinohydrazide}$, 2,4'-Hpcad = N^3 -(2-pyridoyl)-4-

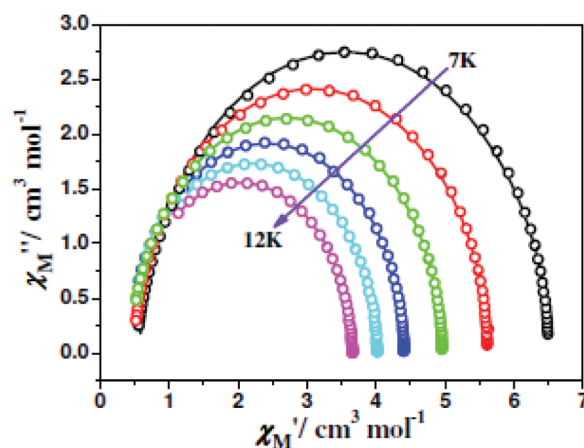


Fig. 11 Cole–Cole plots recorded at 7–12 K under a zero dc field for **2**. The solid lines are the best fits to the experimental data, which were obtained with a generalized Debye model with values of the α parameter of less than 0.05.

pyridinecarboxamidrazone and 2,3'-Hpcad = N^3 -(2-pyridoyl)-3-pyridinecarboxamidrazone. Some salient structural and magnetic parameters of these six compounds are compared in Table 4. Notably, all five compounds 2–6 are SMMs under a zero dc field. However, although both the temperature-dependent out-of-phase and the in-phase ac susceptibilities at different frequencies exhibit maxima for all of 2, 3, 5 and 6, no maximum is observed even in the out-of-phase data for compound 4. The SMM parameters (U_{eff} and τ_0) of 2, 3, 5 and 6, as observed from Arrhenius plots, are: 52.8 cm^{-1} and 1.52×10^{-6} s for 2, 27.2 cm^{-1} and 6.4×10^{-7} s for 3, 37.2 cm^{-1} and 5.7×10^{-6} s for 5 and 92.16 cm^{-1} and 3.8×10^{-7} s for 6.¹² Hence, compound 2 in this investigation may be said to have the second best U_{eff} value among the Dy^{III} compounds with two $\eta^1:\eta^2:\mu_2$ -carboxylate moieties.

An interesting difference in dc magnetic behaviour between 2 and 3–6 is that the former exhibits a rapid increase in $\chi_{\text{M}}T$ values at low temperatures (below 20 K), whereas the latter four compounds exhibit a rapid decrease in $\chi_{\text{M}}T$ values at low temperatures (below *ca.* 20, 30, 15 and 15 K, respectively), *i.e.*, the Dy^{III} centres in 2 are ferromagnetically coupled, but those in the other four compounds are antiferromagnetically coupled.¹² It is worth mentioning that *ab initio* CASSCF calculations for 5 and 6 also reveal the existence of an antiferromagnetic interaction.^{12c} A similar difference is also observed for the Gd^{III} compounds. As already discussed, the Gd^{III} analogue of 2, *i.e.*, 1, exhibits an intramolecular ferromagnetic interaction with $J = 0.021 \text{ cm}^{-1}$. With regard to the other four Dy^{III} compounds (3–6), only the Gd^{III} analogue (7) of 3 was reported, which exhibits an antiferromagnetic interaction with $J = -0.01 \text{ cm}^{-1}$.^{12a}

Although all the Dy^{III} compounds 2–6 have $\eta^1:\eta^2:\mu_2$ -carboxylate moieties, a bis($\mu_{1,1}$ -carboxylate) bridging moiety and a capped square antiprism as the most ideal coordination environment of the lanthanide(III) centre, 2 is most closely comparable with 3 because of the following reasons: (i) both $[\text{Dy}^{\text{III}}\text{L}_2(\text{acetate})_4(\text{MeOH})_2]$ (2) and $[\text{Dy}^{\text{III}}\text{L}^1_2(\text{acetate})_4(\text{MeOH})_2] \cdot 2\text{MeOH}$ (3) have similar inner-sphere compositions (both HL and HL¹ are phenol-hydrazone ligands: the former is the condensation product of 3-ethoxysalicylaldehyde and acetohydrazide and the latter is the condensation product of salicylaldehyde and 2-mercaptocotinothiazide), whereas the composition as well as the types of all/some ligands in 2/3 are different from those in the other three compounds and (ii) the coordination environment of Dy^{III} in both 2 and 3 is NO_8 , which comprises one N(hydrazone), one O(phenoxo), one O(carboxyl), one O(methanol) and five O(acetate) atoms, whereas it is O_9 in 4 and N_2O_7 in 5/6. The respective capped square antiprismatic coordination polyhedra and selected bond lengths and angles in 2 and 3 are compared in Scheme S1 and Tables S3 and S4,[†] respectively. Scheme S1[†] reveals that although similar ligands are present in 2 and 3, there is a remarkable difference in the positions of the ligand atoms. A carboxyl oxygen atom (O2), the non-bridging oxygen atom (O7) of one $\eta^1:\eta^2:\mu_2$ -acetate ligand, the bridging oxygen atom (O8) of the other $\eta^1:\eta^2:\mu_2$ -acetate ligand and a methanol

Table 4 Some structural and magnetic parameters of bis($\eta^1:\eta^2:\mu_2$ -carboxylate) $\text{Ce}^{\text{III}}/\text{Dy}^{\text{III}}$ systems

Components	2	3	4	5 and 6
Environment around Dy^{III} in terms of ligand atoms	$[\text{Dy}^{\text{III}}\text{L}_2(\text{acetate})_4(\text{MeOH})_2]^a$ NO_8 ; N(hydrazone)O(phenoxo)O(carboxyl)O(MeOH)	$[\text{Dy}^{\text{III}}\text{L}^1_2(\text{acetate})_4(\text{MeOH})_2] \cdot 2\text{MeOH}^a$ NO_8 ; N(hydrazone)O(phenoxo)O(carboxyl)O(MeOH)O ₃ (carboxylate, acetate)	$[\text{Dy}^{\text{III}}(n\text{-butyrate})_6(\text{MeOH})_2(\text{H}_2\text{O})_2]$ O_9 ; O ₇ (carboxylate, <i>n</i> -butyrate)O(methanol)O(water)	$[\text{Dy}^{\text{III}}(2,4\text{'-pcad})_2(\text{acetate})_4(\text{H}_2\text{O})_2] \cdot 4\text{H}_2\text{O}$; $[\text{Dy}^{\text{III}}(2,3\text{'-pcad})_2(\text{acetate})_4(\text{H}_2\text{O})_2]$ N_2O_7 ; N(hydrazone)N(pyridine)O(carboxyl)O(water)O ₃ (carboxylate, acetate)
Geometry	Spherical capped square antiprism	Spherical capped square antiprism	Spherical capped square antiprism	Spherical capped square antiprism
Dy–O–Dy angle	115.36°	111.87°	113.1°	113.77° and 112.67°
Magnetic exchange	Ferromagnetic	Antiferromagnetic	Antiferromagnetic	Antiferromagnetic
SMM property	SMM under a zero dc field; $U_{\text{eff}} = 52.8 \text{ cm}^{-1}$	SMM under a zero dc field; $U_{\text{eff}} = 27.2 \text{ cm}^{-1}$	SMM under a zero dc field; no maxima in out-of-phase signals.	SMM under a zero dc field; $U_{\text{eff}} = 37.2 \text{ cm}^{-1}$ (5), 92.2 cm^{-1} (6)
Magnetic exchange in Gd^{III} analogue	Ferromagnetic; $J = 0.02 \text{ cm}^{-1}$	Antiferromagnetic; $J = -0.01 \text{ cm}^{-1}$	Not studied	Not studied
Ref.	This work	12a	12b	12c

^a HL = (E)-N'-(3-ethoxysalicylidene)acetohydrazide; HL¹ = (E)-N'-(2-hydroxybenzylidene)-2-mercaptocotinothiazide.

oxygen atom (O4) define a square plane in **2**, whereas a phenolate oxygen atom (O2), the non-bridging oxygen atom (O5) of one $\eta^1:\eta^2:\mu_2$ -acetate ligand, the bridging oxygen atom (O6A) of the other $\eta^1:\eta^2:\mu_2$ -acetate ligand and a methanol oxygen atom (O7) define a square plane in **3**. The second square plane in **2** is defined by a phenolate oxygen atom (O1), two oxygen atoms (O6 and O5) of η^2 -acetate ligands and a hydrazone nitrogen atom (N1), whereas the equivalent square plane in **3** is defined by a carboxyl oxygen atom (O1), two oxygen atoms (O3 and O4) of η^2 -acetate ligands and a hydrazone nitrogen atom (N3). Clearly, in terms of coordination positions, the carboxyl oxygen atom in **2** is equivalent to the phenolate oxygen atom in **3** and *vice versa*, which, in turn, gives rise to different ligand fields around the lanthanide(III) centre in the two compounds. Although the corresponding metal–ligand bond distances in **2** and **3** are not in general very different (Table S3†), a number of corresponding bond angles are drastically different (Table S4;† the bond angles in **2** and **3** are compared in terms of equivalent coordination positions but not in terms of equivalent ligand atoms; for example, the angles involving the carboxyl oxygen atom in **2** are compared with those involving the phenolate oxygen atom in **3**). It is worth mentioning that similar differences (Scheme S2 and Tables S5 and S6†) also exist between the two corresponding Gd^{III} compounds **1** and **7** (Scheme S3†). It is logical to mention that these remarkable differences between **2** and **3** and between **1** and **7** arise because of a difference in steric factors, which, in turn, arises from the presence of a 2-mercaptopyridine moiety in **3/7** in comparison with a methyl moiety in **2/1**, as well as the presence of an ethoxy moiety in **2/1** in comparison with a hydrogen atom in **3/7**. Hence, the difference in the nature of the magnetic exchange interactions may be qualitatively rationalized in terms of the appreciable differences in the effective ligand field and steric effects in **2/1** in comparison with **3/7**.

Theoretical studies

To get a quantitative and in-depth insight into the nature of the magnetic exchange interactions and magnetic relaxation mechanisms, DFT calculations for compound **1** and *ab initio* CASSCF/RASSI-SO calculations³⁶ for compound **2** (Dy₂^{III}) were undertaken. In addition, *ab initio* calculations were also carried out for the previously reported compounds **3** (Dy₂^{III}) and **4** (Dy₂^{III}) (*ab initio* CASSCF calculations for **5** and **6** were reported previously) using MOLCAS 8.0 software (see the Computational details section in the ESI† for more information).³⁷ The computational protocol that was employed is known to yield good numerical estimates of the anisotropic parameters, as evidenced by earlier studies.³⁸

To determine the mechanism of magnetic relaxation, we initially performed *ab initio* CASSCF/RASSI-SO/SINGLE_ANISO calculations^{36,39} for the individual Dy^{III} ions in compounds **2–4**. For our CASSCF calculations for the single Dy^{III} ions, we used nine electrons in seven active 4f orbitals. Next, in the RASSI-SO step, 21 roots of sextet spin multiplicity were considered. This methodology has a proven track record in ratio-

nalizing, and also at times predicting, reliable mechanisms of magnetic relaxation.^{8b,d,9c,38,40} Then, we used the POLY_ANISO routine in MOLCAS to fit the susceptibility data using the Lines model to determine the magnetic exchange constant and to develop a relaxation mechanism for the exchange-coupled dimer.^{15a,41}

Single-ion magnetic relaxation mechanism. Initially, calculations were performed for single-ion Dy(III) centres, for which we estimated eight lowest-lying Kramer's doublets (KDs) corresponding to ⁶H_{15/2} states, which are estimated to lie in the energy range of 334.0–585.3 cm⁻¹ for compounds **2–4** (see Table S7 in the ESI†). The ground state of complexes **2–4** is estimated to comprise states with $m_j = \pm 15/2$, whereas the first excited state is mixed in nature (Fig. 12). For complexes **2** and **3**, which have equivalent Dy^{III} ions, the gap between the ground and first excited states is estimated to be 99.6 cm⁻¹ and 141.6 cm⁻¹, respectively. The energy gap between the ground-state and first-excited-state KDs is found to be 71.0 cm⁻¹ and 65.5 cm⁻¹ for Dy1 and Dy2, respectively, in complex **4** (Table 5). These results show that the energy gap between the ground and first excited states is significantly larger for complexes **2** and **3**, whereas it is computed to be smaller for complex **4**. Although the energy gap is correlated to the crystal field splitting energy, this suggests that the splitting of the m_j levels in **4** is relatively weaker in comparison with that in **2** and **3**. The computed ground state of complexes **2** and **3** is found to be of a pure Ising nature ($g_{zz} = 19.788$ – 19.870 , $g_{xx} = g_{yy} = 0.005$ – 0.155) (Table 5), which suggests that there is very little operative QTM within the ground-state KD. In contrast, for complex **4** the computed ground state has a relatively larger transverse component ($g_{zz} = 19.253$ – 19.282 , $g_{xx} = g_{yy} = 0.084$ – 0.200 , Table 5). The computed ground state g-anisotropy for the Dy^{III} ions in complexes **2–4** is shown in Fig. 13. The ground states of complexes **2–4** have a very small transverse magnetic component with very little operative quantum tunnelling of magnetization (0.004 – $0.041\mu_B$, Fig. 12). The Orbach/Raman processes related to the ground and first excited states of complex **3** with opposite magnetization are found to be very slight ($0.037\mu_B$, Fig. 12). In contrast, for complexes **2** and **4** these processes are found to be sufficient (0.210 – $0.240\mu_B$, Fig. 12) to cause relaxation *via* the first excited state. The first excited state of the individual Dy^{III} ions in complexes **2–4** is found to have a substantial transverse magnetic component with significant operative TA-QTM (0.130 – $0.89\mu_B$, Fig. 12), which leads to relaxation *via* the first excited state, and the U_{cal} value (Dy1/Dy2) is estimated to be 99.6/99.6 cm⁻¹, 141.6/141.6 cm⁻¹ and 71.0/65.5 cm⁻¹, respectively, for complexes **2–4**. The ratio of the non-axial term (B_k^q , where $q \neq 0$ and $k = 2, 4$ and 6) to the axial term (B_k^q , where $q = 0$ and $k = 2, 4$ and 6) is found to be greater for all the studied complexes (Table S8†), which confirms that there is significant operational QTM in all the studied complexes at the single-ion level.^{38c} This is the likely reason for the observed differences between the U_{cal} and U_{eff} values.

Polynuclear magnetic relaxation mechanism. Experimental studies suggest that complexes **2–4** exhibit zero-field SMM

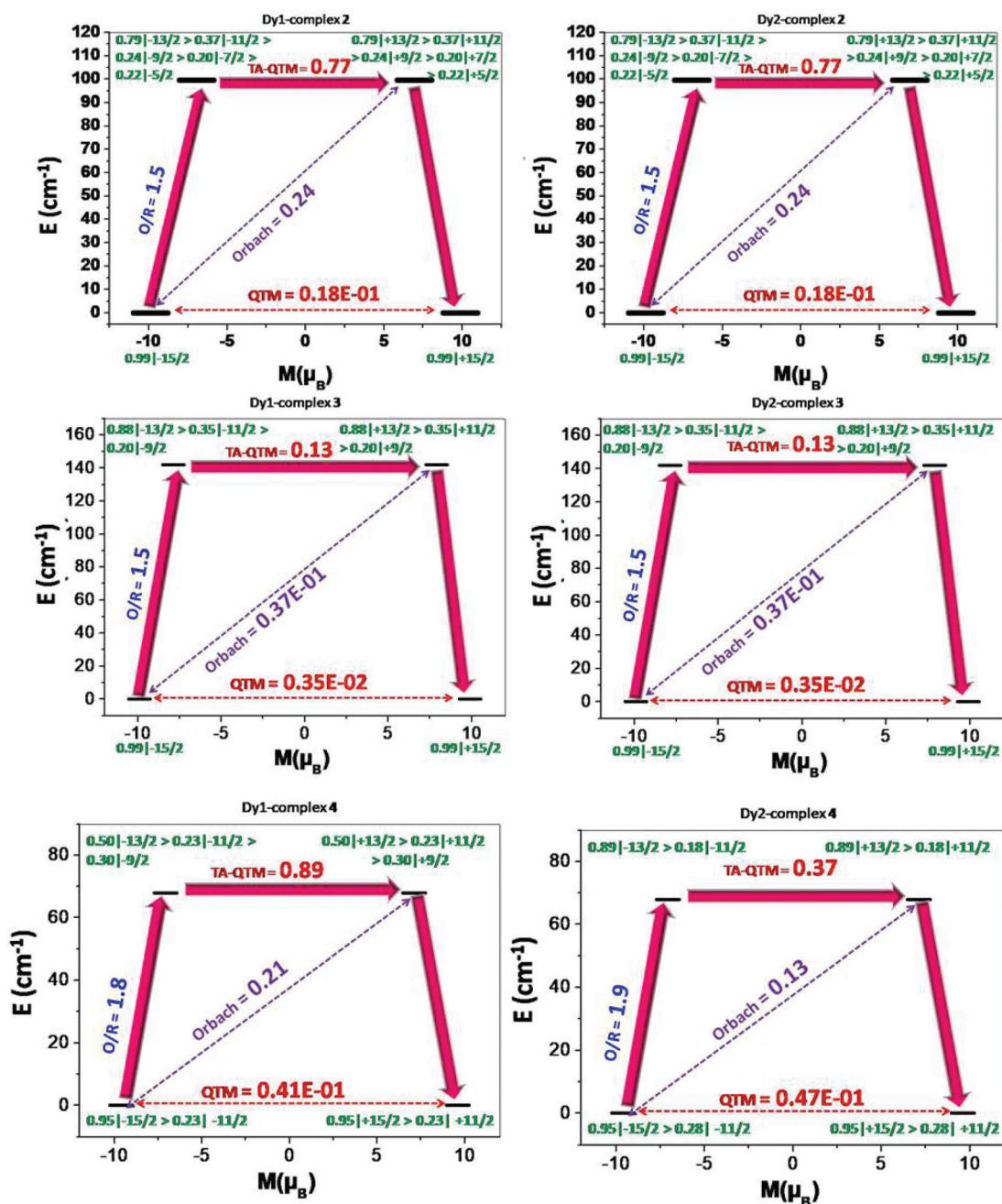


Fig. 12 Magnetization blocking barriers computed *ab initio* for the Dy1 (left) and Dy2 (right) ions in complexes 2–4. The x-axis indicates the magnetic moment of each state along the main magnetic axis of the Dy ions, whereas the y-axis denotes the energy of the respective states. The thick black lines indicate the Kramer's doublets as a function of the computed magnetic moment. The indigo arrows show the possible pathway via Orbach/Raman relaxation. The dotted red lines represent the presence of QTM/TA-QTM between the connecting pairs. The numbers attached to each arrow are the mean absolute values of the corresponding matrix elements of the transition magnetic moment. The numbers given in green correspond to a wavefunction analysis of the M_J levels.

behaviour, but the trend in the magnitude of U_{cal} is not in accordance with the experimental data at the single-ion level, which clearly suggests that the magnetic exchange interaction between the metal ions plays an important role in the mechanism of relaxation. To further investigate the magnetic relaxation at the $\{Dy_2\}$ level and to consider Dy^{III} – Dy^{III} exchange, we

performed POLY_ANISO calculations. By employing all the *ab initio* computed anisotropic parameters, the experimental susceptibility was fitted using a single exchange parameter using the Lines model to obtain the exchange coupling constant. This model has been previously employed to obtain a good numerical estimate of magnetic exchange parameters⁴² and

Table 5 *Ab initio* computed ground state g-tensors together with the energy separation between the ground and first excited states and the angle between the ground-state and first-excited-state KD for both Dy^{III} centres in 2–4

		Dy1	$E_{\text{KD1}}-E_{\text{KD2}}$ (cm ⁻¹)	Angle	Dy2	$E_{\text{KD1}}-E_{\text{KD2}}$ (cm ⁻¹)	Angle
2	$g_{xx\text{KD1}}/g_{xx\text{KD2}}$	0.042/1.279	99.6	31.4	0.042/1.280	99.6	31.4
	$g_{yy\text{KD1}}/g_{yy\text{KD2}}$	0.065/2.404			0.065/2.405		
	$g_{zz\text{KD1}}/g_{zz\text{KD2}}$	19.788/16.279			19.788/16.278		
3	$g_{xx\text{KD1}}/g_{xx\text{KD2}}$	0.005/0.156	141.6	23.7	0.005/0.155	141.6	23.7
	$g_{yy\text{KD1}}/g_{yy\text{KD2}}$	0.016/0.452			0.155/0.451		
	$g_{zz\text{KD1}}/g_{zz\text{KD2}}$	19.870/17.208			19.870/17.225		
4	$g_{xx\text{KD1}}/g_{xx\text{KD2}}$	0.096/1.607	71.0	9.5	0.084/0.810	65.5	12.7
	$g_{yy\text{KD1}}/g_{yy\text{KD2}}$	0.151/3.230			0.200/1.211		
	$g_{zz\text{KD1}}/g_{zz\text{KD2}}$	19.282/14.495			19.253/15.477		

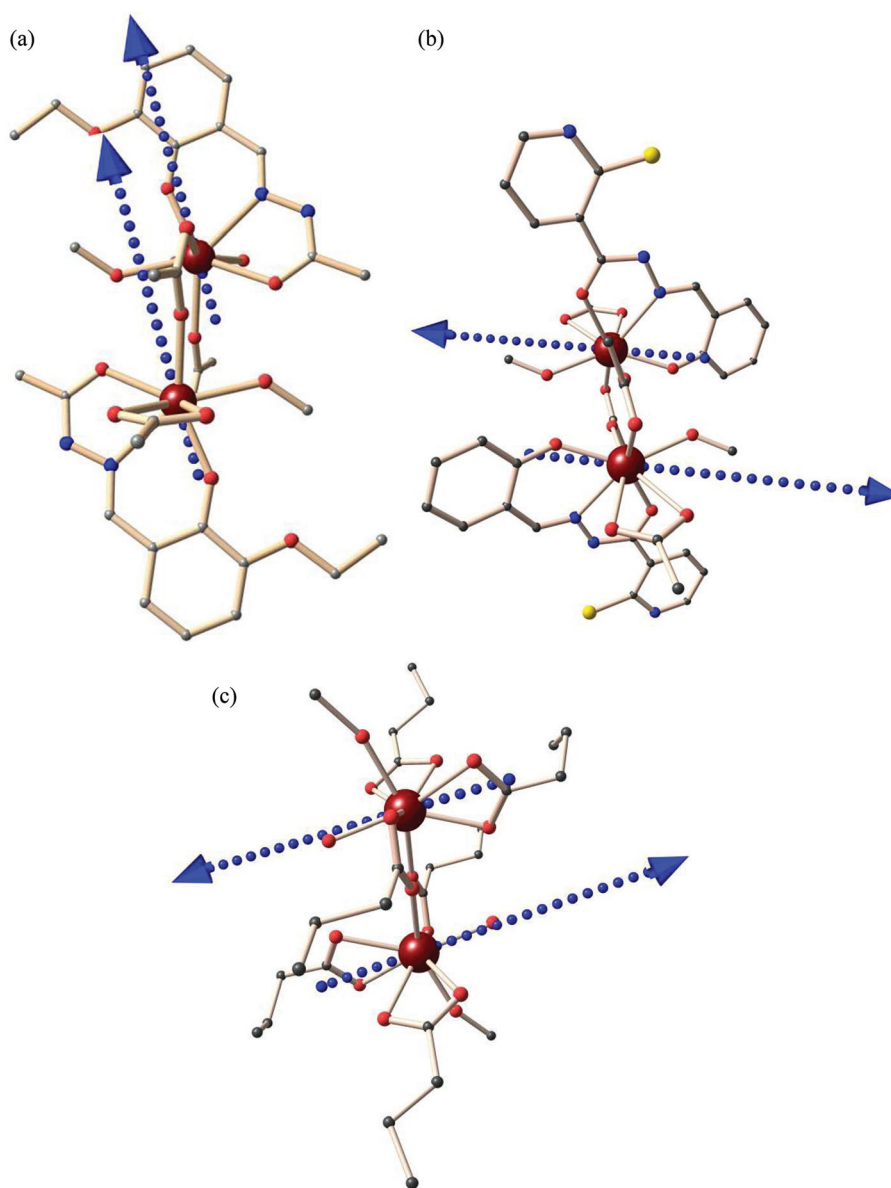


Fig. 13 Directions of the local anisotropy axes in the ground-state Kramer's doublet at the site of each paramagnetic metal (blue dotted lines) in 2 (a), 3 (b) and 4 (c).

has been validated for a range of {3d–4f} dimers by employing exchange coupling constants determined *via* HF-EPR spectroscopy.⁴³ Computed Dy^{III}–Dy^{III} exchange coupling parameters for complexes 2–4 are shown in Table S9 in the ESI† and are in good agreement with the experimental values/plots (Fig. S6†). For complexes 3 and 4, the Dy^{III}–Dy^{III} interaction is found to be weakly antiferromagnetic, whereas for complex 2 this interaction is found to be weakly ferromagnetic in nature. It is important to mention here that the exchange coupling constants (J_{exchange}) fitted using POLY_ANISO for all the complexes are estimated to be small and are ferromagnetic in nature. This is in agreement with established magneto-structural correlations⁴⁴ (see Fig. S7 in the ESI† for more information). The dipolar contribution to the coupling constant (J_{dipolar}) for complex 2 is estimated to be ferromagnetic. For complexes 3 and 4, J_{dipolar} is estimated to be antiferromagnetic in nature. For complexes 2–4, the value of J_{dipolar} is found to be larger than the value of J_{exchange} , which yields a total magnetic coupling constant (J_{total}) that is ferromagnetic ($J_{\text{total}} = J_{\text{exchange}} + J_{\text{dipolar}}$) for complex 2 and antiferromagnetic for complexes 3 and 4. Besides, a spin density plot computed *via* DFT for complex 1 also suggests that the magnitude of the magnetic interaction between both Gd^{III} ions is small (Fig. S8†).

For complexes 2 and 3, the tunnelling parameter (Δ_{tun}) for the exchange-coupled ground state is computed to be small (9.7×10^{-6} and 2.7×10^{-7} , respectively, Fig. 14a and b). In complex 2, the first excited state has a relatively large tunnelling parameter ($\Delta_{\text{tun}} = 1.8 \times 10^{-4}$), which suggests relaxation *via* the first excited state with a U_{cal} value of 99.6 cm^{-1} (Fig. 14a). The tunnelling splitting computed for the exchange-coupled ground state of complex 2 is on the borderline, which suggests the possibility of relaxation *via* this state; however, weak intermolecular interactions/other factors may suppress this QTM to enforce relaxation *via* the first excited state lying at 99.6 cm^{-1} . Because ground-state QTM is not expected to be completely quenched, a great difference between the values of U_{cal} and U_{eff} is expected, as is observed here. This picture is consistent with the experimental data, from which a relaxation process is observed with a barrier height of 52.8 cm^{-1} (experimental) in the absence of an external magnetic field. It is important to note here that the deviation between the computed and experimental susceptibility plots for complex 2 (Fig. 5) is attributed to a strong intermolecular interaction ($\text{NH}\cdots\text{O} = 2.734 \text{ \AA}$), which is either absent or very weak in complexes 3 and 4.

In complex 3, relaxation is expected to occur *via* the first excited state (0.4 cm^{-1} above the ground state), which has an

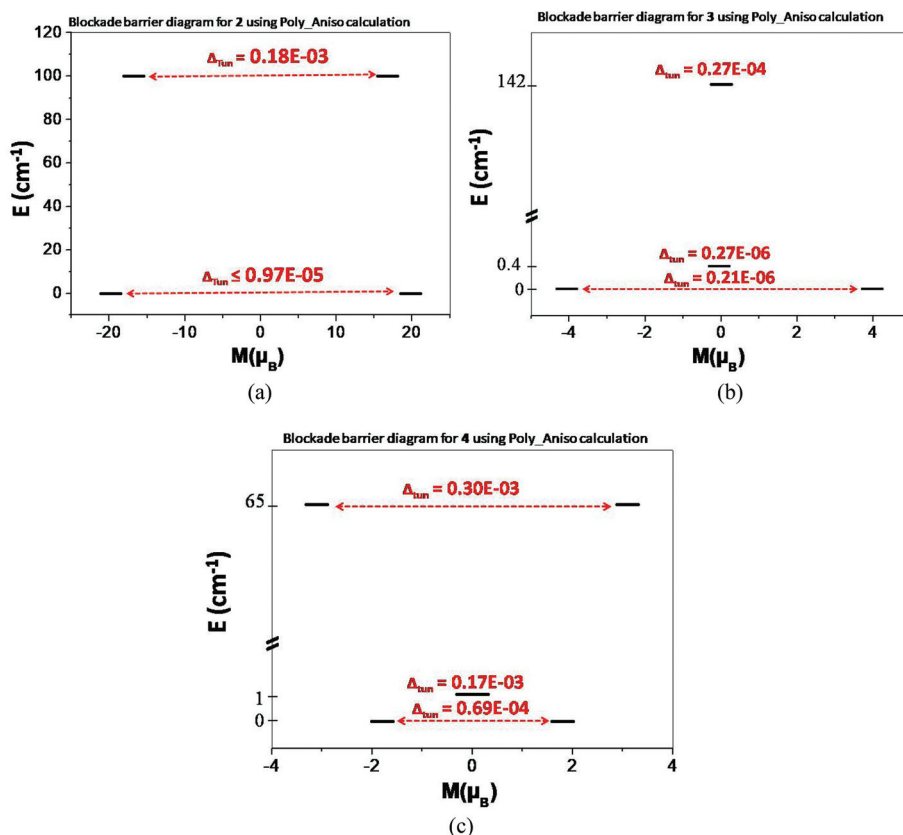


Fig. 14 Magnetization blocking barriers computed *ab initio* using POLY_ANISO for complexes 2–4, shown as (a), (b) and (c), respectively. The x-axis indicates the magnetic moment of each state along the main magnetic axis of the Dy^{III} ions, whereas the y-axis denotes the energy of the respective states. The thick black line indicates the Kramer's doublets as a function of the computed magnetic moment. The dotted red lines represent the presence of QTM/TA-QTM between the connecting pairs. The numbers provided are the mean absolute values of the corresponding matrix elements of the transition magnetic moment.

m_j value of $\pm 1/2$ because of weakly antiferromagnetic Dy^{III}-Dy^{III} coupling. However, the tunnelling splitting of the ground state is very small and hence results in magnetization blockage; because the first excited state is extremely close (at a distance of 0.4 cm^{-1}) at the temperature at which the measurements were performed ($\sim 2 \text{ K}$), one can expect partial population of the second excited state (at 141 cm^{-1}), which will lead to a small but significant blockade barrier. This is the likely reason for the smaller U_{eff} value (27.2 cm^{-1}) for complex **3** in comparison with that for complex **2**. For complex **4**, the tunnelling parameters (Δ_{tun}) for the exchange-coupled ground state and first excited state, which lies $\sim 1 \text{ cm}^{-1}$ above the ground state, are estimated to be 6.9×10^{-5} and 1.7×10^{-4} , respectively (Fig. 14), which suggests zero-field SMM behaviour with a very small effective barrier, which fits well with the experiments, in which complex **4** was found to exhibit only tails in the out-of-phase signals at zero field. SHAPE analysis gives a trend of $4 > 3 > 2$ for the distortion of Dy^{III} ions with respect to the ideal spherical capped square antiprismatic geometry, which is the reverse to that in the estimated $U_{\text{cal}}/U_{\text{eff}}$ values (Table S10†). A previous study by Gao *et al.*⁴⁵ suggests an increase in the QTM rate with an increase in the distortion from the ideal square antiprismatic geometry because of a significant increase in the transverse anisotropy, which is closely correlated with our findings. Very recently, a magneto-structural correlation in this context has been undertaken for several mononuclear Dy(III) molecules, and this study reiterates the respective findings.⁴⁶

Conclusions

The two title bis($\eta^1:\eta^2$; μ_2 -acetate)Gd^{III}/Dy^{III} compounds of the formula $[\text{Ln}^{\text{III}}\text{L}_2(\text{acetate})_4(\text{MeOH})_2]$ (**1**, Ln = Gd; **2**, Ln = Dy) are among only a few examples of dinuclear lanthanide compounds that have such a bridging moiety. Interestingly, whereas all previously reported bis($\eta^1:\eta^2$; μ_2 -acetate)Gd^{III}/Dy^{III} compounds exhibit antiferromagnetic interactions, the metal centres in both **1** and **2** are ferromagnetically coupled, which has been rationalized by DFT/*ab initio* calculations for **1**, **2** and two other previously reported Dy^{III} compounds (**3** and **4**). Clearly, this study represents a rare case of the transition from antiferromagnetic to ferromagnetic exchange interactions in lanthanide compounds with similar bridging moieties.

The single-ion relaxation mechanism in *ab initio* calculations reveals very little QTM within the ground-state KD but prominent TA-QTM via the first-excited-state KD in all of **2–4**. However, the order of the U_{eff} values of **2–4** does not match the order of the U_{cal} values; the U_{eff} value of **2** (52.8 cm^{-1}) is greater than that of **3** (27.2 cm^{-1}), but the U_{cal} value of **2** (99.6 cm^{-1}) is smaller than that of **3** (141.6 cm^{-1}). This anomaly, interestingly, can be rationalized by taking into account the magnetic interaction and polynuclear magnetic relaxation mechanism. The relatively high (1.8×10^{-4}) tunnelling parameter of the ferromagnetically coupled first excited state of **2** facilitates appreciable QTM via this state. In contrast, the antiferromagnetically coupled first excited state of **3** is very

close in energy to the ground state (energy gap = 0.4 cm^{-1}), and therefore partial population of the second excited state (at 141 cm^{-1}) takes place, which provides a small but sufficient blockade barrier, which, in turn, is responsible for a smaller anisotropic barrier.

Conflicts of interest

There are no conflicts to declare.

Acknowledgements

Financial support for this work has been received from the Government of India through the University Grants Commission (contingency from CAS-V project to S. M.), the Council of Scientific and Industrial Research (fellowship to S. G.) and the Department of Science and Technology (INSPIRE fellowship to S. Mandal). Crystallography was performed at the DST-FIST-funded Single Crystal Diffractometer Facility at the Department of Chemistry, University of Calcutta. The Centre for Research in Nanoscience and Nanotechnology (CRNN), University of Calcutta, is acknowledged for magnetic data (in Fig. 4, 5, 6, S3 and S4). G. R. thanks the SERB (EMR/2014/00024) and INSA for funding. M. K. S. thanks UGC-India for fellowship. C.-M. L. acknowledges the funding from the National Natural Science Foundation of China (21471154).

References

- (a) W. E. Wallace, *Prog. Solid State Chem.*, 1985, **16**, 127; (b) R. J. Radwanska, R. Michalskia, Z. Ropkaa and A. Blaut, *Phys. B: Condens. Matter*, 2002, **319**, 78; (c) J. D. Rinehart and J. R. Long, *Chem. Sci.*, 2011, **2**, 2078; (d) L. Sorace, C. Benelli and D. Gatteschi, *Chem. Soc. Rev.*, 2011, **40**, 3092.
- N. Ishikawa, M. Sugita, T. Ishikawa, S. Koshihara and Y. Kaizu, *J. Am. Chem. Soc.*, 2003, **125**, 8694.
- (a) R. Sessoli, D. Gatteschi, A. Caneschi and M. A. Novak, *Nature*, 1993, **365**, 141; (b) D. Gatteschi, R. Sessoli and J. Villain, *Molecular Nanomagnets*, Oxford Univ. Press, 2006; (c) *Struct. Bonding*, ed. R. E. Winpenny, 2006, vol. 122, p. 1; (d) T. C. Stamatatos and G. Christou, *Inorg. Chem.*, 2009, **48**, 3308; (e) S. Mukherjee, K. A. Abboud, W. Wernsdorfer and G. Christou, *Inorg. Chem.*, 2013, **52**, 873; (f) M. Murrie, *Chem. Soc. Rev.*, 2010, **39**, 1986; (g) I. G. Rau, S. Baumann, S. Rusponi, F. Donati, S. Stepanow, L. Gragnaniello, J. Dreiser, C. Piamonteze, F. Nolting, S. Gangopadhyay, O. R. Albertini, R. M. Macfarlane, C. P. Lutz, B. A. Jones, P. Gambardella, A. J. Heinrich and H. Brune, *Science*, 2014, **344**, 988; (h) S. A. Corrales, J. M. Cain, K. A. Uhlig, A. M. Mowson, C. Papatriantafyllopoulou, M. K. Peprah, A. Ozarowski, A. J. Tasiopoulos, G. Christou, M. W. Meisel and C. Lampropoulos, *Inorg. Chem.*, 2016, **55**, 1367; (i) S. Mandal, S. Mondal, C. Rajnák, J. Titiš, R. Boča and S. Mohanta, *Dalton Trans.*, 2017, **46**, 13135; (j) G. A. Craig

- and M. Murrie, *Chem. Soc. Rev.*, 2015, **44**, 2135;
- (k) M. Murrie, *Chem. Soc. Rev.*, 2010, **39**, 1986.
- 4 (a) L. Bogani and W. Wernsdorfer, *Nat. Mater.*, 2008, **7**, 179;
- (b) E. Coronado and A. J. Epsetin, *J. Mater. Chem.*, 2009, **19**, 1670.
- 5 (a) M. Shiddiq, D. Komijani, Y. Duan, A. Gaita-Ariño, E. Coronado and S. Hill, *Nature*, 2016, **531**, 348;
- (b) M. N. Leuenberger and D. Loss, *Nature*, 2001, **410**, 789.
- 6 (a) D. Gatteschi, *Adv. Mater.*, 1994, **6**, 635; (b) F. Donati, S. Rusponi, S. Stepanow, C. Wäckerlin, A. Singha, L. Persichetti, R. Baltic, K. Diller, F. Patthey, E. Fernandes, J. Dreiser, Z. Šljivančanin, K. Kummer, C. Nistor, P. Gambardella and H. Brune, *Science*, 2016, **352**, 318.
- 7 (a) D. N. Woodruff, R. E. P. Winpenny and R. A. Layfield, *Chem. Rev.*, 2013, **113**, 5110; (b) R. J. Holmberg and M. Murugesu, *J. Mater. Chem. C*, 2015, **3**, 11986;
- (c) Y.-S. Meng, S.-D. Jiang, B.-W. Wang and S. Gao, *Acc. Chem. Res.*, 2016, **49**, 2381; (d) S. T. Liddle and J. V. Slagereen, *Chem. Soc. Rev.*, 2015, **44**, 6655; (e) K. Liu, X. Zhang, X. Meng, W. Shi, P. Chengab and A. K. Powell, *Chem. Soc. Rev.*, 2016, **45**, 2423; (f) Y.-N. Guo, G.-F. Xu, Y. Guo and J. Tang, *Dalton Trans.*, 2011, **40**, 9953;
- (g) R. Sessoli and A. K. Powell, *Coord. Chem. Rev.*, 2009, **253**, 2328; (h) P. Zhang, L. Zhang and J. Tang, *Dalton Trans.*, 2015, **44**, 3923; (i) J. Lu, M. Guo and J. Tang, *Chem. – Asian J.*, 2017, **12**, 2772; (j) Z. Zhu, M. Guo, X.-L. Li and J. Tang, *Coord. Chem. Rev.*, DOI: 10.1016/j.ccr.2017.10.030.
- 8 (a) C. A. P. Goodwin, F. Ortu, D. Reta, N. F. Chilton and D. P. Mills, *Nature*, 2017, **548**, 439; (b) S. K. Gupta, T. Rajeshkumar, G. Rajaraman and R. Murugavel, *Chem. Sci.*, 2016, **7**, 5181; (c) F. S. Guo, B.-M. Day, Y.-C. Chen, M.-L. Tong, A. Mansikkamaki and R. A. Layfield, *Angew. Chem., Int. Ed.*, 2017, **56**, 11445; (d) Y.-C. Chen, J.-L. Liu, L. Ungur, J. Liu, Q.-W. Li, L.-F. Wang, Z.-P. Ni, L. F. Chibotaru, X.-M. Chen and M.-L. Tong, *J. Am. Chem. Soc.*, 2016, **138**, 2829.
- 9 (a) J. D. Rinehart, M. Fang, W. J. Evans and J. R. Long, *J. Am. Chem. Soc.*, 2011, **133**, 14236; (b) J. J. L. Roy, L. Ungur, I. Korobkov, L. F. Chibotaru and M. Murugesu, *J. Am. Chem. Soc.*, 2014, **136**, 8003; (c) J. Liu, Y.-C. Chen, J.-L. Liu, V. Vieru, L. Ungur, J.-H. Jia, L. F. Chibotaru, Y. Lan, W. Wernsdorfer, S. Gao, X.-M. Chen and M.-L. Tong, *J. Am. Chem. Soc.*, 2016, **138**, 5441.
- 10 (a) J. Ruiz, A. J. Mota, A. Rodríguez-Diéguez, S. Titos, J. M. Herrera, E. Ruiz, E. Cremades, J. P. Costes and E. Colacio, *Chem. Commun.*, 2012, **48**, 7916; (b) A. B. Canaj, M. K. Singh, C. Wilson, G. Rajaraman and M. Murrie, *Chem. Commun.*, 2018, **54**, 8273.
- 11 (a) J. Long, F. Habib, P.-H. Lin, I. Korobkov, G. Enright, L. Ungur, W. Wernsdorfer, L. F. Chibotaru and M. Murugesu, *J. Am. Chem. Soc.*, 2011, **133**, 5319;
- (b) F. Habib, G. Brunet, V. Vieru, I. Korobkov, L. F. Chibotaru and M. Murugesu, *J. Am. Chem. Soc.*, 2013, **135**, 13242; (c) S. Xue, Y.-N. Guo, L. Ungur, J. Tang and L. F. Chibotaru, *Chem. – Eur. J.*, 2015, **21**, 14099;
- (d) L. Zhang, J. Jung, P. Zhang, M. Guo, L. Zhao, J. Tang and B. L. Guennic, *Chem. – Eur. J.*, 2016, **22**, 1392;
- (e) Y. Peng, V. Mereacre, A. Baniodeh, Y. Lan, M. Schlageter, G. E. Kostakis and A. K. Powell, *Inorg. Chem.*, 2016, **55**, 68;
- (f) P. Comba, M. Großhauser, R. Klingeler, C. Koo, Y. Lan, D. Müller, J. Park, A. K. Powell, M. J. Riley and H. Wadepohl, *Inorg. Chem.*, 2015, **54**, 11247; (g) E. C. Mazarakioti, J. Regier, L. Cunha-Silva, W. Wernsdorfer, M. Pilkington, J. Tang and T. C. Stamatatos, *Inorg. Chem.*, 2017, **56**, 3568;
- (h) Y.-Z. Zheng, Y. Lan, W. Wernsdorfer, C. E. Anson and A. K. Powell, *Chem. – Eur. J.*, 2009, **15**, 12566.
- 12 (a) H. Zhang, S.-Y. Lin, S. Xue, C. Wanga and J. Tang, *Dalton Trans.*, 2014, **43**, 6262; (b) B. Joarder, A. K. Chaudhari, G. Rogezb and S. K. Ghosh, *Dalton Trans.*, 2012, **41**, 7695; (c) L. Sun, S. Wei, J. Zhang, W. Wang, S. Chen, Y. Zhang, Q. Wei, G. Xie and S. Gao, *J. Mater. Chem. C*, 2017, **5**, 9488.
- 13 (a) Y.-L. Wang, C.-B. Han, Y.-Q. Zhang, Q.-Y. Liu, C.-M. Liu and S.-G. Yin, *Inorg. Chem.*, 2016, **55**, 5578; (b) Y.-B. Lu, X.-M. Jiang, S.-D. Zhu, Z.-Y. Du, C.-M. Liu, Y.-R. Xie and L.-X. Liu, *Inorg. Chem.*, 2016, **55**, 3738; (c) G. Huang, X. Yi, J. Jung, O. Guillou, O. Cadour, F. Pointillart, B. Le Guennic and K. Bernot, *Eur. J. Inorg. Chem.*, 2018, 326; (d) I. Cimatti, X. Yi, R. Sessoli, M. Puget, B. Le Guennic, J. Jung, T. Guizouarn, A. Magnani, K. Bernot and M. Mannini, *Appl. Surf. Sci.*, 2018, **432**, 7.
- 14 M.-J. Liu, J. Yuan, J. Tao, Y.-Q. Zhang, C.-M. Liu and H.-Z. Kou, *Inorg. Chem.*, 2018, **57**, 4061.
- 15 (a) L. F. Chibotaru, L. Ungur and A. Soncini, *Angew. Chem., Int. Ed.*, 2008, **47**, 4126; (b) I. F. Díaz-Ortega, J. M. Herrera, T. Gupta, G. Rajaraman, H. Nojiri and E. Colacio, *Inorg. Chem.*, 2017, **56**, 5594.
- 16 (a) C. Das, S. Vaidya, T. Gupta, J. M. Frost, M. Righi, E. K. Brechin, M. Affronte, G. Rajaraman and M. Shanmugam, *Chem. – Eur. J.*, 2015, **21**, 15639;
- (b) S. Biswas, S. Das, T. Gupta, S. K. Singh, M. Pissas, G. Rajaraman and V. Chandrasekhar, *Chem. – Eur. J.*, 2016, **22**, 18532.
- 17 (a) R. J. Blagg, C. A. Muryn, E. J. L. McInnes, F. Tuna and R. E. P. Winpenny, *Angew. Chem., Int. Ed.*, 2011, **50**, 6530;
- (b) M. T. Gamer, Y. Lan, P. W. Roesky, A. K. Powell and R. Clérac, *Inorg. Chem.*, 2008, **47**, 6581.
- 18 I. J. Hewitt, J. Tang, N. T. Madhu, C. E. Anson, Y. Lan, J. Luzon, M. Etienne, R. Sessoli and A. K. Powell, *Angew. Chem., Int. Ed.*, 2010, **49**, 6352.
- 19 (a) S. Das, A. Dey, S. Kundu, S. Biswas, R. S. Narayanan, S. Titos-Padilla, G. Lorusso, M. Evangelisti, E. Colacio and V. Chandrasekhar, *Chem. – Eur. J.*, 2015, **21**, 16955;
- (b) S. Biswas, S. Das, J. Acharya, V. Kumar, J. V. Leusen, P. Kögerler, J. M. Herrera, E. Colacio and V. Chandrasekhar, *Chem. – Eur. J.*, 2017, **23**, 5154;
- (c) S. Biswas, J. Chakraborty, V. S. Parmar, S. P. Bera, N. Ganguli and S. Konar, *Inorg. Chem.*, 2017, **56**, 4956;
- (d) S. Biswas, H. S. Jena, A. Adhikary and S. Konar, *Inorg. Chem.*, 2014, **53**, 3926; (e) R.-P. Li, Q.-Y. Liu, Y.-L. Wang, C.-M. Liu and S.-J. Liu, *Inorg. Chem. Front.*, 2017, **4**, 1149;
- (f) G. Huang, G. Fernandez-Garcia, I. Badiane, M. Camarra,

- S. Freslon, O. Guillou, C. Daignebonne, F. Totti, O. Cador, T. Guizouarn, B. Le Guennic and K. Bernot, *Chem. – Eur. J.*, 2018, **24**, 6983.
- 20 (a) K. R. Vignesh, S. K. Langley, K. S. Murray and G. Rajaraman, *Inorg. Chem.*, 2017, **56**, 2518; (b) J. Goura, J. Brambleby, P. Goddard and V. Chandrasekhar, *Chem. – Eur. J.*, 2015, **21**, 4926; (c) S. Hazra, J. Titiš, D. Valigura, R. Boča and S. Mohanta, *Dalton Trans.*, 2016, **45**, 7510.
- 21 J. Goura, A. Chakraborty, J. P. S. Walsh, F. Tuna and V. Chandrasekhar, *Cryst. Growth Des.*, 2015, **15**, 3157.
- 22 (a) M. M. Hänninen, A. J. Mota, R. Sillanpää, S. Dey, G. Velmurugan, G. Rajaraman and E. Colacio, *Inorg. Chem.*, 2018, **57**, 3683; (b) K. R. Vignesh, S. K. Langley, B. Mobaraki, K. S. Murray and G. Rajaraman, *Chem. – Eur. J.*, 2015, **21**, 16364.
- 23 D. Schray, G. Abbas, Y. Lan, V. Mereacre, A. Sundt, J. Dreiser, O. Waldmann, G. E. Kostakis, C. E. Anson and A. K. Powell, *Angew. Chem.*, 2010, **122**, 5312.
- 24 (a) K. R. Vignesh, A. Soncini, S. K. Langley, W. Wernsdorfer, K. S. Murray and G. Rajaraman, *Nat. Commun.*, 2017, **8**, 1023; (b) K. R. Vignesh, S. K. Langley, A. Swain, B. Mobaraki, M. Damjanović, W. Wernsdorfer, G. Rajaraman and K. S. Murray, *Angew. Chem., Int. Ed.*, 2018, **57**, 779.
- 25 (a) M. J. H. Ojea, V. A. Milway, G. Velmurugan, L. H. Thomas, S. J. Coles, C. Wilson, W. Wernsdorfer, G. Rajaraman and M. Murrie, *Chem. – Eur. J.*, 2016, **22**, 12839; (b) D. I. Alexandropoulos, K. M. Poole, L. Cunha-Silva, J. A. Sheikh, W. Wernsdorfer, G. Christou and T. C. Stamatatos, *Chem. Commun.*, 2017, **53**, 4266.
- 26 N. Ahmed, C. Das, S. Vaidya, S. K. Langley, K. S. Murray and M. Shanmugam, *Chem. – Eur. J.*, 2014, **20**, 14235.
- 27 O. Kahn, *Molecular Magnetism*, VCH Publications, New York, 1993.
- 28 (a) S. Hazra, S. Bhattacharya, M. K. Singh, L. Carrella, E. Rentschler, T. Weyhermueller, G. Rajaraman and S. Mohanta, *Inorg. Chem.*, 2013, **52**, 12881; (b) S. Sasmal, S. Roy, L. Carrella, A. Jana, E. Rentschler and S. Mohanta, *Eur. J. Inorg. Chem.*, 2015, 680; (c) S. Sasmal, S. Hazra, P. Kundu, S. Dutta, G. Rajaraman, E. C. Sañudo and S. Mohanta, *Inorg. Chem.*, 2011, **50**, 7257; (d) S. Mohanta, K. K. Nanda, L. K. Thompson, U. Flo1rke and K. Nag, *Inorg. Chem.*, 1998, **37**, 1465.
- 29 E. Ruiz, J. Cano, S. Alvarez and P. Alemany, *J. Am. Chem. Soc.*, 1998, **120**, 11122.
- 30 J.-P. Costes, F. Dahan and A. Dupuis, *Inorg. Chem.*, 2000, **39**, 165.
- 31 (a) L. E. Roy and T. Hughbanks, *J. Am. Chem. Soc.*, 2006, **128**, 568; (b) G. Rajaraman, F. Totti, A. Bencini, A. Caneschi, R. Sessoli and D. Gatteschi, *Dalton Trans.*, 2009, 3153; (c) S. K. Singh, N. K. Tibrewal and G. Rajaraman, *Dalton Trans.*, 2011, **40**, 10897; (d) T. Rajeshkumar and G. Rajaraman, *Chem. Commun.*, 2012, **48**, 7856; (e) M. K. Singh, T. Rajeshkumar, R. Kumar, S. K. Singh and G. Rajaraman, *Inorg. Chem.*, 2018, **57**, 1846.
- 32 K. Zhang, D. Liu, V. Vieru, L. Hou, B. Cui, F.-S. Guo, L. F. Chibotaru and Y.-Y. Wang, *Dalton Trans.*, 2017, **46**, 638.
- 33 (a) Bruker–Nonius 2004, APEX-II, SAINT-Plus and TWINABS. Bruker–Nonius AXS Inc., Madison, Wisconsin, USA; (b) G. M. Sheldrick, SAINT (Version 6.02), SADABS, (Version 2.03), Bruker AXS Inc., Madison, Wisconsin, 2002; (c) G. M. Sheldrick, SHELXS-97, Crystal Structure Solution Program, University of Göttingen, 2008; (d) G. M. Sheldrick, SHELXL-2014/7, Crystal Structure Refinement Program, University of Göttingen, 2014.
- 34 (a) J. Cirera, E. Ruiz and S. Alvarez, *Chem. – Eur. J.*, 2006, **12**, 3162; (b) M. Pinsk and D. Avnir, *Inorg. Chem.*, 1998, **37**, 5575.
- 35 N. F. Chilton, R. P. Anderson, L. D. Turner, A. Soncini and K. S. Murray, *J. Comput. Chem.*, 2013, **34**, 1164–1175.
- 36 (a) B. Swerts, L. F. Chibotaru, R. Lindh, L. Seijo, Z. Barandiaran, S. Clima, K. Pierloot and M. F. A. Hendrickx, *J. Chem. Theory Comput.*, 2008, **4**, 586; (b) P. Å. Malmqvist, B. O. Roos and B. Schimmelpfennig, *Chem. Phys. Lett.*, 2002, **357**, 230.
- 37 (a) F. Aquilante, J. Autschbach, R. K. Carlson, L. F. Chibotaru, M. G. Delcey, L. De Vico, I. F. Galvan, N. Ferre, L. M. Frutos, L. Gagliardi, M. Garavelli, A. Giussani, C. E. Hoyer, G. L. Manni, H. Lischka, D. Ma, P. Å. Malmqvist, T. Muller, A. Nenov, M. Olivucci, T. B. Pedersen, D. Peng, F. Plasser, B. Pritchard, M. Reiher, I. Rivalta, I. Schapiro, J. Segarra-Martí, M. Stenrup, D. G. Truhlar, L. Ungur, A. Valentini, S. Vancoillie, V. Veryazov, V. P. Vysotskiy, O. Weingart, F. Zapata and R. Lindh, *J. Comput. Chem.*, 2016, **37**, 506; (b) J. A. Duncan, *J. Am. Chem. Soc.*, 2009, **131**, 2416; (c) V. Veryazov, P. O. Widmark, L. Serrano-Andrés, R. Lindh and B. O. Roos, *Int. J. Quantum Chem.*, 2004, **100**, 626; (d) F. Aquilante, L. D. Vico, N. Ferré, G. Ghigo, P.-Å. Malmqvist, P. Neogrady, T. B. Pedersen, M. Pitoňák, M. Reiher, B. O. Roos, L. Serrano-Andrés, M. Urban, V. Veryazov and R. Lindh, *J. Comput. Chem.*, 2010, **31**, 224; (e) G. Karlström, R. Lindh, P.-Å. Malmqvist, B. O. Roos, U. Ryde, V. Veryazov, P.-O. Widmark, M. Cossi, B. Schimmelpfennig, P. Neogrady and L. Seijo, *Comput. Mater. Sci.*, 2003, **28**, 222.
- 38 (a) M. K. Singh and G. Rajaraman, *Chem. Commun.*, 2016, **52**, 14047; (b) M. K. Singh, N. Yadav and G. Rajaraman, *Chem. Commun.*, 2015, **51**, 17732; (c) A. K. Bar, P. Kalita, M. K. Singh, G. Rajaraman and V. Chandrasekhar, *Coord. Chem. Rev.*, 2018, **367**, 163.
- 39 (a) L. F. Chibotaru and L. Ungur, *J. Chem. Phys.*, 2012, **137**, 064112; (b) L. F. Chibotaru, A. Ceulemans and H. Bolvin, *Phys. Rev. Lett.*, 2008, **101**, 033003.
- 40 (a) Y.-S. Ding, N. F. Chilton, R. E. P. Winpenny and Y.-Z. Zheng, *Angew. Chem., Int. Ed.*, 2016, **55**, 16071; (b) J. L. Liu, Y. C. Chen, Y. Z. Zheng, W. Q. Lin, L. Ungur, W. Wernsdorfer, L. F. Chibotaru and M. L. Tong, *Chem. Sci.*, 2013, **4**, 3310; (c) S. K. Singh, T. Gupta and G. Rajaraman, *Inorg. Chem.*, 2014, **53**, 10835; (d) S. K. Singh, T. Gupta, M. Shanmugam and G. Rajaraman, *Chem. Commun.*, 2014, **50**, 15513.

- 41 (a) L. Ungur, W. Van den Heuvel and L. F. Chibotaru, *New J. Chem.*, 2009, **33**, 1224; (b) L. F. Chibotaru, L. Ungur, C. Aronica, H. Elmoll, G. Pilet and D. Luneau, *J. Am. Chem. Soc.*, 2008, **130**, 12445.
- 42 M. E. Lines, *J. Chem. Phys.*, 1971, **55**, 2977.
- 43 T. Gupta, M. F. Beg and G. Rajaraman, *Inorg. Chem.*, 2016, **55**, 11201.
- 44 T. Rajeshkumar, S. K. Singh and G. Rajaraman, *Polyhedron*, 2013, **52**, 1299.
- 45 Y. Bi, Y.-N. Guo, L. Zhao, Y. Guo, S.-Y. Lin, S.-D. Jiang, J. Tang, B.-W. Wang and S. Gao, *Chem. – Eur. J.*, 2011, **17**, 12476.
- 46 T. Gupta and G. Rajaraman, *Eur. J. Inorg. Chem.*, DOI: 10.1002/ejic.201800350.